Particle
& Particle Systems Characterization
www.particle-journal.com

Materials Views
www.MaterialsViews.com

Quantitative Structure Determination of Large Three-Dimensional Nanoparticle Assemblies

*Thomas Altantzis, Bart Goris, Ana Sánchez-Iglesias, Marek Grzelczak, Luis M. Liz-Marzán, and Sara Bals**

Self-assembly of nanoparticles has recently received increasing interest[1] because it is an attractive route towards systems in which the properties can be tuned using parameters such as the size of the individual particles and the nature of their three-dimensional (3D) stacking. However, in order to understand the structure/property relationship, a thorough characterization of the nanoparticle organization is of crucial importance. Although conventional transmission electron microscopy (TEM) is a very useful tool to study nanoscale materials, it only provides two-dimensional (2D) projection images of a 3D object. Therefore, electron tomography has become a standard technique in the 3D characterization of nanomaterials. In electron tomography, 2D projection images acquired using a TEM are combined into a 3D reconstruction through a mathematical algorithm.

Several groups have demonstrated the ability to investigate nanoparticle assemblies by electron tomography.[2,3] In those cases, either bright field TEM (BF-TEM) or high angle annular dark field scanning TEM (HAADF-STEM) was used to obtain the series of 2D images. However, if one wants to extract quantitative information, optimization of the electron tomography experiment is required. This is especially the case for large assemblies that have a thickness >500 nm. For such systems, the conventional approaches yield different types of artifacts hampering a quantitative interpretation of the 3D data. Here, we propose an improved route towards the quantitative structure determination of large 3D nanoparticle assemblies, which required optimization of both the acquisition technique and the reconstruction algorithm. We demonstrate that this approach is of crucial importance in the investigation of so-called "superspheres", containing Au nanoparticles stabilized by a polymer matrix. Because they have a large diameter and contain no specific features that can hamper a reliable reconstruction, these large assemblies serve as good test objects to investigate the influence of both the acquisition technique and the reconstruction algorithm on the quality of the reconstruction. Such systems have also become of high importance in the field of nanoplasmonics because they may lead to controlled hot spot formation and antenna effects.[4] By changing the size of the individual nanoparticles and the length of the polymer chains, different 3D structures can be obtained that require detailed characterization.

Colloidal superspheres were prepared using a recently reported procedure.[5] Briefly, gold nanoparticle building blocks (20 and 40 nm diameter) were stabilized with hydrophobic polymer (thiolated polystyrene, molecular weight = 53 000 g/mol). The length of the polymer chains was determined by dynamic light scattering to be 39 nm and 45 nm for gold nanoparticles with diameter of 20 nm and 40 nm respectively, indicating different chain conformations for particles with different curvature. The polystyrene-stabilized particles spontaneously self-assemble in a THF/H_2O mixture and the assemblies can be stabilized within polymeric micelles of a diblock copolymer (polystyrene-*block*-poly acrylic acid). The final size of the assemblies in solution was 160 nm ± 4 nm and 670 nm ± 10 nm for 20 and 40 nm gold nanoparticles, respectively. TEM samples were prepared by drop casting the aqueous solution of the assemblies on holey, carbon-coated copper grids.

Electron tomography experiments were carried out using a Tecnai G20 Electron Microscope, operated at 200 kV. A Fischione tomography holder (model 2020) was used and the series were acquired automatically using the Xplore3D software. All tilt series were acquired in STEM mode with an angular range from –76° to +70° and a tilt increment of 2°. For the illumination system, a probe semiconvergence angle was used that equals 16 mrad, corresponding to a depth of focus of approximately 70 nm. As discussed below, the camera length and therefore the collection angle of the annular detector were optimized according to the samples to be investigated. The alignment of the series was done by a combination of Inspect 3D software, provided by FEI, and manual alignment using the IMOD software.[6] 3D reconstruction was performed using the simultaneous iterative reconstructive technique (SIRT) as implemented in Inspect3D. A more advanced method for the 3D reconstruction, the so-called "total variation minimization" approach for electron tomography is explained in more detail with the results. The visualization of all the reconstructions was done using the Amira 5.4.0 software package from Mercury Computer Systems.

Although many approaches exist,[7–12] electron tomography in materials science is performed in most cases using HAADF-STEM. The reason is related to the unwanted diffraction contrast in BF-TEM mode that hampers the "projection requirement" in tomography, which states that the intensity in each projection image of a tilt series should be a monotonic function of a certain property of the sample under investigation. When using HAADF-STEM, the signal scales with the thickness of the sample. In addition, the signal is proportional to Z^n

T. Altantzis, B. Goris, Prof. S. Bals
EMAT, University of Antwerp
Groenenborgerlaan 171, B-2020 Antwerp, Belgium
E-mail: Sara.Bals@ua.ac.be
A. Sánchez-Iglesias, Dr. M. Grzelczak,
Prof. L. M. Liz-Marzán
Departamento de Química Física
Universidade de Vigo, 36310 Vigo, Spain

DOI: 10.1002/ppsc.201200045

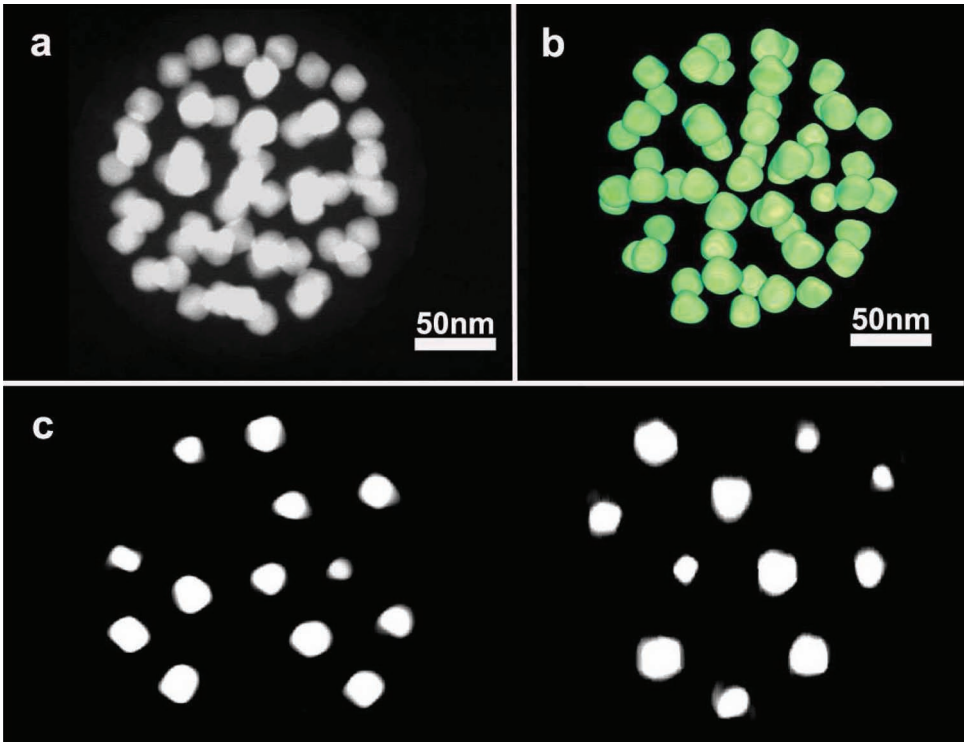

Figure 1. a) HAADF STEM image of a relatively small assembly of Au particles at a 0° tilt angle. b) Volume rendering of the reconstructed supersphere. c) Two different orthoslices through the reconstructed volume, showing that the gray levels are the same for all particles.

($1.6 < n < 2$).[10,13,14] We used HAADF-STEM to visualize the 3D structure of an assembly consisting of 20 nm Au particles and 39 nm long polymer chains. The total diameter of the assembly is 160 nm ± 4 nm. In **Figure 1**a, a 2D projection HAADF-STEM image of the structure is presented. Diffraction contrast was avoided by setting the inner semi collection angle of the detector to 90 mrad. A tilt series of images was acquired and used as an input for a tomographic reconstruction based on the SIRT algorithm. During the reconstruction, an optimized number of 30 iterations was used as proposed by Mezerji et al.[15] to obtain a 3D reconstruction. The result of the procedure is illustrated in Figure 1b, where a volume rendering of the structure is shown. Two different orthoslices through the 3D reconstruction are also presented in Figure 1c. It can be seen that the gray level is equal for all particles, including those present in the middle of the assembly. Based on the HAADF-STEM technique, this is exactly what is to be expected since all particles contain only the chemical element Au.

Next, an assembly with a larger total diameter was investigated. In this case, the diameter of the assembly was found to be equal to 670 nm ± 10 nm, with individual particle sizes of 40 nm and the length of the polymer chains being 45 nm. Also for this cluster, HAADF-STEM was used with the inner semicollection angle of the detector being 90 mrad and SIRT algorithm of 30 iterations was used for the tomographic reconstruction. A 2D projection image of the structure is presented in Supporting Information Figure S1a and orthoslices, as well as a volume rendering of the structure, are presented in **Figures 2**a and **3**a, respectively. Although the volume rendering can be interpreted in a qualitative manner, the orthoslice in Figure 2a shows that not all reconstructed particles yield the same gray level. An underestimation of the intensity is found in the central part of the assembly. This is due to the so-called "cupping artifact", which is related to the thickness of the assembly and the high atomic number of Au. This results in an increase of multiple scattering and backscattering as was discussed previously.[16] Consequently, a smaller amount of the incoming electron beam is scattered towards the detector, leading to an underestimation of the intensity. The cupping artifact clearly affects the reconstruction of the particles at the inner shells of this assembly. As a consequence, both qualitative and quantitative interpretations of the results are no longer straightforward. In particular, a quantitative interpretation will be hampered: when quantifying a 3D reconstruction, one needs to carry out a segmentation step in which a correspondence is defined between certain gray scales or features in the original sample and specific gray scales or features in the 3D reconstruction. Due to the cupping artifact, the nanoparticles at the inner part of the assembly will have a different gray level from those at the outside. This will complicate the segmentation and therefore the quantification of the results.

A partial solution to overcome this problem is the use of a technique referred to as incoherent bright field STEM (IBF-STEM).[17,18] This technique has been used successfully for electron tomography of thick samples in the past.[19–21] Since the IBF-STEM signal is incoherent, it scales with the atomic

Particle
& Particle Systems Characterization
www.particle-journal.com

Materials Views
www.MaterialsViews.com

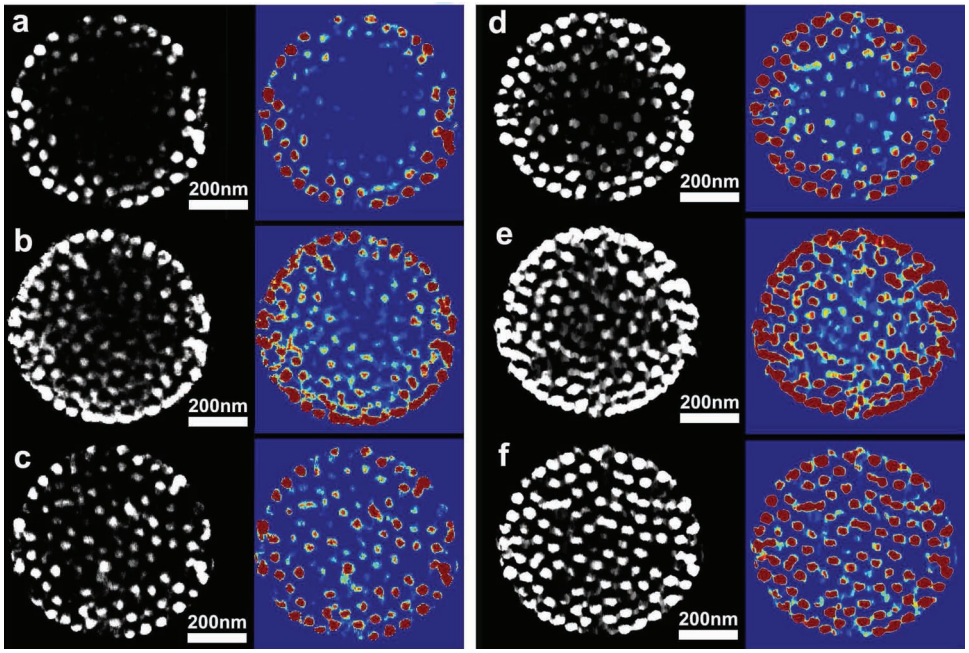

Figure 2. Orthoslices (obtained orthogonal to the incoming electron beam at 0° tilt angle) of the reconstructed volumes based on a tilt series of either HAADF-STEM, IBF-STEM and corrected IBF-STEM combined with a SIRT reconstruction (a–c) or with a TVM reconstruction (d–f). Color maps are presented to facilitate the visualization of the cupping artifacts that are present in the HAADF-STEM and the non-corrected IBF-STEM tilt series. For these color maps, the intensity is scaled between an arbitrary minimum value (blue) and a maximum value (red).

number Z of the elements present in the sample and the thickness of the sample.[19,22] IBF-STEM was used to obtain a tilt series of the same assembly as shown in Supporting Information Figure S1b. When acquiring this series, the inner semicollection angle of the detector was several times larger than the beam's convergence semiangle, in order to preserve the incoherent imaging.[19] A schematic overview of the experimental set-up can be found in the Supporting Information (Figure S2). Using this set-up, electrons scattered between 0–90 mrads are collected.[19] When using the raw IBF-STEM projection images,

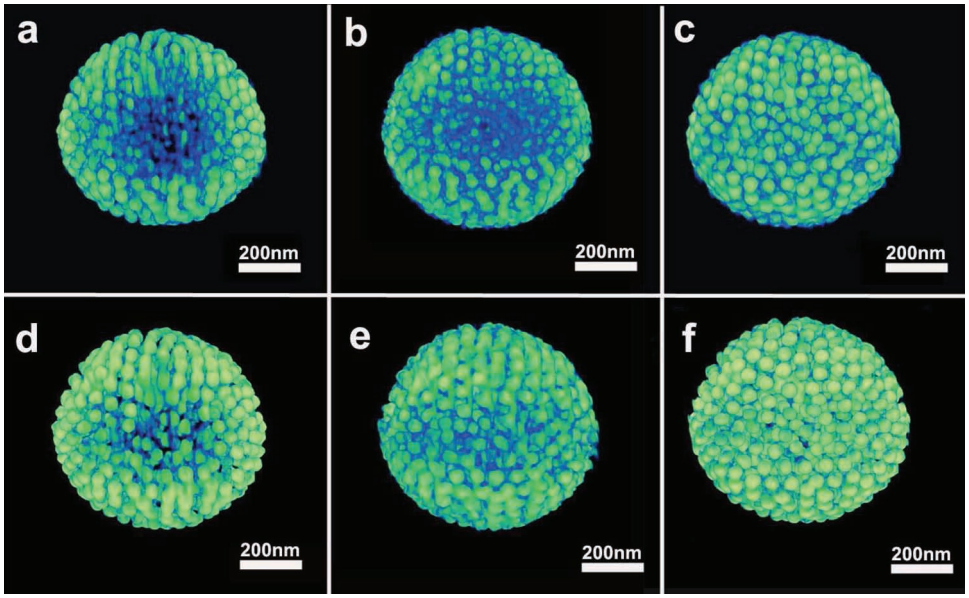

Figure 3. Volume renderings of a relatively large assembly based on a tilt series of HAADF-STEM, IBF-STEM and corrected IBF-STEM projections and reconstructed with either a SIRT algorithm (a–c) or a TVM algorithm (d–f). It can be seen that a combination of corrected IBF-STEM projections with a TVM reconstruction algorithm renders the best result.

the cupping artifact can still be expected, due to Beer's law (Figures 2b and 3b). Therefore a correction for this artifact has been applied.[16]

The intensity I' that is scattered to angles smaller than θ_{in} (see Supporting Information Figure S1) and which is collected by the detector when using IBF STEM, is shown to decrease exponentially as a function of object thickness t:

$$I' = I_o \exp(-\mu t) \text{ with } \mu = \eta \sigma \quad (1)$$

In this expression, I_o is the intensity of the beam as it enters the object, η is the number of atoms per unit of volume, σ is the Rutherford scattering cross section to angles larger than θ_{in} and μ is defined as the attenuation coefficient and equals the inverse of the mean free path between scattering events. Instead of using the raw IBF STEM images yielding intensity I', images with corrected intensities equal to $-\ln(I'/I_o)$ were used for further reconstruction. The intensity, I_o, can be estimated from a projection of a region containing no specimen, where the recorded signal equals the intensity of the incoming electron beam.

The result of a SIRT reconstruction is presented in Figure 2c (orthoslice) and Figure 3c (volume rendering). It can be seen that the nanoparticles in the middle of the assembly yield now a gray value that is closer to the ones observed at the outer part of the assembly, but still, a straightforward segmentation is not possible due to remaining artifacts in the final reconstruction. This motivates the optimization of the reconstruction technique as well.

For electron tomography reconstructions in materials science, weighted backprojection (WBP) or SIRT are the most commonly used reconstruction algorithms.[23] The use of SIRT to reconstruct the small assembly (Figure 1a) was found to be adequate, but for the large assembly, the reconstructions appear with a low signal-to-noise ratio (Figure 3a,b,c). In addition, the effect of the so-called "missing wedge", due to the limited tilt range during the experiment becomes more obvious.[10,24] Recently, new algorithms were proposed in which the quality of a reconstruction can be drastically improved.[25–30] Here, we will use the total variation minimization technique (TVM), which is based on compressive sensing.[31–34] It is hereby assumed that the object that needs to be reconstructed has a sparse gradient. For objects at the nanoscale this is often a valid assumption and the advantages of using compressive sensing for electron tomography were demonstrated for different nanostructures already.[28–30] The technical details of the technique can be found in the Supporting Information.

TVM reconstructions were carried out for the large assembly using the HAADF-STEM series, the uncorrected IBF-STEM series and the corrected IBF-STEM series. The results of the orthoslices are shown in Figure 2d–f and those of the volume rendering are presented in Figure 3d–f. It is clear that the combination of HAADF-STEM and TVM yields better results in comparison to all reconstructions based on the SIRT algorithm. However, it is only when combining TVM and IBF-STEM with the corrections of the intensity that a reconstruction is obtained in which segmentation can be carried out in a straightforward manner. This can be clearly observed from the orthoslices and the corresponding scaled color maps in Figure 2f, where all the particles in the volume have the same gray value. It must be noted that no artifacts are observed in this visualization that could be caused by the limited depth of focus during the acquisition of the projection images. Using this reconstruction, a segmentation based on a single threshold becomes straightforward. As a consequence, also quantification becomes possible leading to interesting information about the particle distribution in the assembly. For example, in this case we were able to determine the number of particles in each reconstruction. In case a segmentation (using the same threshold value) is performed for the HAADF-STEM series, reconstructed using SIRT, a total number of 70 segmented particles is found. When segmenting the series acquired by IBF-STEM (corrected for the cupping artifact) and reconstructed using TVM the total number of segmented particles equals 302. This difference (see also Supporting Information Table 1), clearly indicates the importance of our optimized approach in the field of reliable quantification of 3D volumes obtained by electron tomography.

In conclusion, we have shown that 3D quantitative results for large nanoparticle assemblies can be obtained by optimizing different aspects of the electron tomography experiment. For the acquisition, HAADF-STEM imaging is less suited and IBF-STEM imaging, corrected for the so-called cupping artifact presents the best alternative. The total variation minimization technique is presented as the most optimal approach for the 3D reconstruction. Using this methodology, we are able to reconstruct a large (>500 nm) spherical assembly of Au nanoparticles while minimizing any artifacts in the reconstruction. As a result, quantitative information can be obtained in a straightforward manner.

Supporting Information

Supporting Information is available from the Wiley Online Library or from the author.

Acknowledgements

T.A. and S.B. acknowledge the GOA program of the University of Antwerpen. B.G. acknowledges the Flemish Fund for Scientific Research (FWO Vlaanderen)). L.M.L.-M. acknowledges funding from the European Research Council (ERC Advanced Grant 267867 - PLASMAQUO). The authors appreciate financial support from the European Union under the Seventh Framework Program (Integrated Infrastructure Initiative N. 262348 European Soft Matter Infrastructure, ESMI).

Received: July 29, 2012
Revised: September 7, 2012

[1] M. Grzelczak, J. Vermant, E. M. Furst, L. M. Liz-Marzán, *ACS Nano* **2010**, *4*, 3591–3605.
[2] H. Friedrich, C. J. Gommes, K. Overgaag, J. D. Meeldijk, W. H. Evers, B. de Nijs, M. P. Boneschanscher, P. E. de Jongh, A. J. Verkleij, K. P. de Jong, A. van Blaaderen, D. Vanmaekelbergh, *Nano Lett.* **2009**, *9*, 2719–2724.
[3] I. Florea, A. Demortiere, C. Petit, H. Bulou, C. Hirlimann, O. Ersen, *ACS Nano* **2012**, *6*, 2574-2581.

[4] J. M. Romo-Herrera, R. A. Alvarez-Puebla, L. M. Liz-Marzán, *Nanoscale* **2011**, *3*, 1304-1315.
[5] M. Grzelczak, A. Sánchez-Iglesias, H. H. Mezerji, S. Bals, J. Pérez-Juste, L. M. Liz-Marzán, *Nano Lett.* **2012**, *12*, 4380–4384.
[6] J. R. Kremer, D. N. Mastronarde, J. R. McIntosh, *J. Struct. Biol.* **1996**, *116*, 71–76.
[7] B. Goris, S. Bals, W. Van den Broek, J. Verbeeck, G. Van Tendeloo, *Ultramicroscopy* **2011**, *111*, 1262–1267.
[8] S. Bals, G. Van Tendeloo, C. Kisielowski, *Adv. Mater.* **2006**, *18*, 892–895.
[9] A. J. Koster, U. Ziese, A. J. Verkleij, A. H. Janssen, K. P. de Jong, *J. Phys. Chem. B* **2000**, *104*, 9368–9370.
[10] P. A. Midgley, M. Weyland, *Ultramicroscopy* **2003**, *96*, 413–431.
[11] P. A. Midgley, R. E. Dunin-Borkowski, *Nat. Mater.* **2009**, *8*, 271–280.
[12] H. Friedrich, M. R. McCartney, P. R. Buseck, *Ultramicroscopy* **2005**, *106*, 18–27.
[13] P. W. Hawkes, in *Electron Tomography, Three dimensional imaging with the transmission electron microscope*, (Ed: J. Frank), Plenum Press, **1992**, pp. 17–38 Chapter 2.
[14] S. J. Pennycook, *Annu. Rev. Mater. Sci.* **1992**, *22*, 171–195.
[15] H. Heidari Mezerji, W. Van den Broek, S. Bals, *Ultramicroscopy* **2011**, *111*, 330–336.
[16] W. Van den Broek, A. Rosenauer, B. Goris, G. T. Martinez, S. Bals, S. Van Aert, D. Van Dyck, *Ultramicroscopy* **2012**, *116*, 8–12.
[17] Z. H. Levine, *Appl. Phys. Lett.* **2003**, *82*, 3943–3945.
[18] Z. H. Levine, *J. Appl. Phys.* **2005**, *97*, 033101.
[19] P. Ercius, M. Weyland, D. A. Muller, *Appl. Phys. Lett.* **2006**, *88*, 243116.
[20] H. L. Xin, Y. Zhu, D. A. Muller, *Microsc. Microanal.* **2012**, *18*, 720–727.
[21] P. Ercius, L. M. Gignac, C.-K. Hu, D. A. Muller, *Microsc. Microanal.* **2009**, *15*, 244–250.
[22] E. J. Kirkland, R. F. Loane, J. Silcox, *Ultramicroscopy* **1987**, *23*, 77–96.
[23] P. Gilbert, *J. Theor. Biol.* **1972**, *36*, 105–107.
[24] M. Weyland, *Top. Catal.* **2002**, *21*, 175–183.
[25] K. J. Batenburg, S. Bals, J. Sijbers, C. Kubel, P. A. Midgley, J. C. Hernandez, U. Kaiser, E. R. Encina, E. A. Coronado, G. Van Tendeloo, *Ultramicroscopy* **2009**, *109*, 730–740.
[26] E. Biermans, L. Molina, K. J. Batenburg, S. Bals, G. Van Tendeloo, *Nano Lett.* **2010**, *10*, 5014–5019.
[27] S. Bals, K. J. Batenburg, J. Verbeeck, J. Sijbers, G. Van Tendeloo, *Nano Lett.* **2007**, *7*, 3669–3674.
[28] B. Goris, W. Van den Broek, K. J. Batenburg, H. Heidari Mezerji, S. Bals, *Ultramicroscopy* **2012**, *113*, 120–130.
[29] B. Goris, T. Roelandts, K. J. Batenburg, H. Heidari Mezerji, S. Bals, *Ultramicroscopy* DOI. 10.1016/j.ultramic.2012.07.003.
[30] Z. Saghi, D. J. Holland, R. Leary, A. Falqui, G. Bertoni, A. J. Sederman, L. F. Gladden, P. A. Midgley, *Nano Lett.* **2011**, *11*, 4666–4673.
[31] D. Donoho, *Commun. Pure Appl. Anal.* **2006**, *59*, 797–829.
[32] D. Donoho, *IEEE Trans. Inform. Theory* **2006**, *52*, 1289–1306.
[33] E. Candes, J. Romberg, T. Tao, *Commun. Pure Appl. Math.* **2008**, *59*, 1207–1223.
[34] E. Candes, M. Wakin, *IEEE Signal Processing Mag.* **2008**, *25*, 21–30.